PHYSICAL SCIENCES

Molecular structure of bottlebrush polymers in melts

Jarosław Paturej,[1,2,3] Sergei S. Sheiko,[2] Sergey Panyukov,[4] Michael Rubinstein[2]*

Bottlebrushes are fascinating macromolecules that display an intriguing combination of molecular and particulate features having vital implications in both living and synthetic systems, such as cartilage and ultrasoft elastomers. However, the progress in practical applications is impeded by the lack of knowledge about the hierarchic organization of both individual bottlebrushes and their assemblies. We delineate fundamental correlations between molecular architecture, mesoscopic conformation, and macroscopic properties of polymer melts. Numerical simulations corroborate theoretical predictions for the effect of grafting density and side-chain length on the dimensions and rigidity of bottlebrushes, which effectively behave as a melt of flexible filaments. These findings provide quantitative guidelines for the design of novel materials that allow architectural tuning of their properties in a broad range without changing chemical composition.

INTRODUCTION

Significant progress in polymerization techniques allows synthesis of hyperbranched molecules with precisely controlled architectures (*1*–*9*). Dense branching results in distinct shape of individual molecules and reduces overlap of neighboring molecules in dense systems (concentrated solutions and melts). These unique features inspire the design of new materials with physical properties that are different from properties of conventional linear polymers. Branched macromolecules were explored as molecular pressure sensors (*10*), pH-sensitive probes (*11*), supersoft elastomers (*12*, *13*), and drug delivery agents (*14*–*16*). They have also been used as components for the construction of mesoscopic systems (*6*) and controlling conformations of polymer chains (*17*).

One of the most distinct examples of highly branched macromolecules are molecular bottlebrushes composed of many polymer side chains densely grafted to a linear chain (backbone) (Fig. 1). The high grafting density results in strong steric repulsion between the side chains, causing extension of the backbone (*18*–*21*) and, in some cases, even scission of its covalent bonds (*21*, *22*). Because of this steric repulsion, bottlebrushes adapt a wormlike conformation controlled by side-chain length and grafting density (*23*). In bulk melts, this conformation promotes reduction of entanglement density of the wormlike molecules (*24*), resulting in unusual rheological properties (*25*, *26*) with an ultralow plateau modulus of 10^2 to 10^3 Pa (*13*, *25*, *27*), which is much lower than the 10^5 to 10^6 Pa typically observed in melts of linear polymers. Note that these fundamental changes in physical properties are achieved only through architectural control without changing the chemical composition. Varying length and grafting density of side chains allows for systematic control of conformation of individual molecules as well as overlap and entanglements with neighboring molecules in dense systems.

Given their unique physical properties, molecular bottlebrushes have been an active field for many theoretical (*18*, *28*–*32*), experimental (*13*, *27*, *33*–*40*), and numerical investigations (*20*, *22*, *34*, *36*, *41*–*51*). Most of these studies focused on basic structural properties of bottlebrushes in solutions and in the adsorbed state. Particular attention was paid to the bending rigidity of bottlebrush macromolecules, which is characterized by the persistence length ℓ_p and remains a matter of debate in the scientific literature. The major difficulty is the interplay between many length scales in the bottlebrush structure and their impact on ℓ_p. Several theoretical approaches have been proposed to address this problem using scaling analysis (*28*, *29*, *31*, *52*) and the self-consistent field method (*49*). For bottlebrushes in dilute solutions, under good solvent conditions, the persistence length was predicted to scale as $\ell_p \propto N_{sc}^{\alpha}$, with α as low as $^3/_4$ (*28*) or as high as 1.11 (*49*) and $^{15}/_8$ (*29*). The exponent α for bottlebrushes in a θ solvent was predicted to be $^2/_3$ (*28*) or 1.01 (*49*). Significantly less attention has been paid to solvent-free systems (*53*). Here, we address the problem of architecture-induced increase of bottlebrush persistence length as the key feature underlying physical properties of bottlebrush melts and elastomers.

In this work, we present the results of systematic coarse-grained molecular dynamics simulations and scaling analysis of the equilibrium

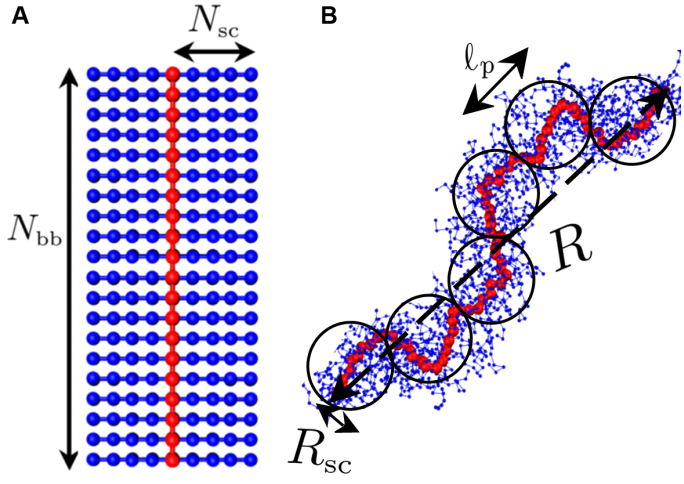

Fig. 1. Molecular architecture and conformation of a bottlebrush polymer. (**A**) Architecture of a bottlebrush molecule consisting of a backbone with N_{bb} monomers (red beads) and z side chains (blue beads) per backbone monomer. Each side chain is made of N_{sc} monomers. The total number of monomers of bottlebrush macromolecule is $N = N_{bb}(1 + zN_{sc})$. All beads in the simulation are considered to be identical and interact via bonded and nonbonded potential (see Materials and Methods for details). Here, $N_{bb} = 20$, $N_{sc} = 4$, and $z = 2$. (**B**) The bottlebrush molecule in a melt state can be represented as a chain of effective persistence segments of length ℓ_p and thickness R_{sc}. R denotes end-to-end distance of bottlebrush backbone. Here, $N_{bb} = 150$, $N_{sc} = 10$, and $z = 2$.

[1]Leibniz Institute of Polymer Research Dresden, 01069 Dresden, Germany. [2]Department of Chemistry, University of North Carolina, Chapel Hill, NC 27599–3290, USA. [3]Institute of Physics, University of Szczecin, 70451 Szczecin, Poland. [4]P.N. Lebedev Physics Institute, Russian Academy of Sciences, Moscow 117924, Russia.
*Corresponding author. Email: mr@unc.edu

structure of bottlebrush polymer melts for a range of degrees of polymerization of the backbone N_{bb}, side chains N_{sc}, and backbone spacer between the neighboring side chains. The latter is inversely proportional to the grafting density z, which is the number of side chains per backbone monomer. We show that the persistence length ℓ_p for $z = 1$ and $z = 2$ bottlebrushes is on the order of the size of side chains $\langle R_{sc}^2\rangle^{1/2}$ and scales as $\ell_p \propto \langle R_{sc}^2\rangle^{1/2} \propto N_{sc}^{1/2}$. This finding suggests that the entanglement plateau modulus of bottlebrush melts decreases as (*27*) $G_e \propto 1/V_{perv} \approx 1/\langle R_{sc}^2\rangle^{3/2} \propto N_{sc}^{-3/2}$, where V_{perv} is the volume of the effective bottlebrush Kuhn segment proportional to the pervaded volume of a side chain $V_{perv} \approx \langle R_{sc}^2\rangle^{3/2}$. The pervaded volume V_{perv} of a side chain is the volume of a sphere that encompasses this side chain. Our results also indicate that the backbones of bottlebrushes for $z = 1$ and $z = 2$ in a melt state obey Gaussian statistics with their size R (root mean square radius of gyration and end-to-end distance) scaling as $\langle R^2\rangle^{1/2} \propto N_{bb}^{1/2} N_{sc}^{1/4}$ for $N_{bb} \gg N_{sc}$. Furthermore, our molecular modeling provided vital insights into the internal organization of bottlebrush melts, including limited interpenetration of side chains of neighboring molecules, radial distribution function of backbone monomers, and the form factor of individual bottlebrushes inside melt. We conclude that bottlebrush melts behave as melts of thick and flexible filaments, with a persistence length proportional to the size of the side chains.

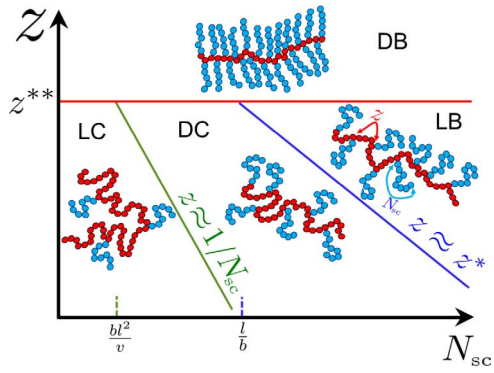

Fig. 2. Diagram of states of combs and bottlebrush molecules. Molecular conformations are determined by the degree of polymerization N_{sc} of side chains (blue circles) and the number z of side chains per backbone monomer (red circles). Four conformational regimes are distinguished: loosely grafted comb-like polymer (LC) with $z < 1/N_{sc}$, densely grafted comb (DC) with $1/N_{sc} < z < z^*$, loosely grafted bottlebrush (LB) with $z^* < z < z^{**}$, and densely grafted bottlebrush (DB) with $z > z^{**}$ (see Eqs. 1 and 3 for the definitions of z^* and z^{**}). The solid lines indicate crossovers between regimes [green, LC-DC boundary at $z \approx 1/N_{sc}$; blue, DC-LB crossover line at $z = z^* = (bl)^{3/2}/(vN_{sc}^{1/2})$; red, LB-DB boundary at z^{**} (see Eq. 3)].

RESULTS

Scaling theory of combs and bottlebrush molecules

Conformations of combs and bottlebrushes depend on the degree of polymerization of the side chains N_{sc} and their grafting density z. Although most of the paper concentrates on bottlebrushes with $z \geq 1$, in the present section, we consider a broader set of parameters, including loosely grafted bottlebrushes (LBs) and loosely grafted combs (LCs) with $z < 1$. Depending on grafting density, we identify four conformational regimes of comb and bottlebrush melts (*27*), depicted in Fig. 2. At lower grafting density, we distinguish two comblike regimes characterized by Gaussian conformations of both backbone and side chains: (i) loosely grafted combs (LCs) with long backbone spacers between side chains $z < 1/N_{sc}$ and with strongly interpenetrating neighboring molecules and (ii) densely grafted combs (DCs) for $1/N_{sc} < z < z^*$ with weak interpenetration between molecules, where z^* is defined in Eq. 1 below. There are also two regimes at higher grafting density: (iii) loosely grafted bottlebrushes (LBs) with extended backbones and Gaussian side chains for intermediate grafting density $z^* < z < z^{**}$ and (iv) densely grafted bottlebrushes (DBs) with extended backbones and side chains for high grafting density of side chains $z > z^{**}$, where z^{**} is defined in Eq. 3 below. The boundary between the comb and bottlebrush regimes can be found from the space-filling condition of zN_{sc} side chains with physical volume vN_{sc}, each within their pervaded volume $(blN_{sc})^{3/2}$, resulting in reduced interpenetration of side chains from neighboring molecules

$$z^* \approx \frac{(bl)^{3/2}}{v} N_{sc}^{-1/2} \quad (1)$$

where b is the Kuhn length, l is the monomer length, and v is the monomer volume. The present paper focuses on the melts of densely grafted bottlebrushes, whereas below we briefly review conformations of other types of molecules.

The low grafting density regime with $z < z^*$ (combs) includes two subregimes: LC and DC. Loosely grafted combs (LC part of Fig. 2), with spacers between side chains longer than the side chains ($z < 1/N_{sc}$) and a high volume fraction of backbones (> 50%), fully interpenetrate each other in melts. Densely grafted combs (DC part of Fig. 2), with spacers shorter than the side chains $1/N_{sc} < z < z^*$, allow only partial interpenetration of the side chains because there is not enough space to accommodate side chains of neighboring molecules near the backbone of a host molecule. Both the side chains and backbones in melts of combs (LC and DC regimes) are in almost unperturbed Gaussian conformations.

Macromolecules with $z > z^*$ correspond to the so-called bottlebrush regime, which onsets because of a lack of space for side chains emanating from the unperturbed Gaussian backbone. Interpenetration of these side chains without their significant deformation is only possible upon extension of the backbone. We can estimate z^* (Eq. 1) by considering a side chain with an unperturbed Gaussian size $\langle R_{sc,0}^2\rangle^{1/2} \approx (blN_{sc})^{1/2}$ and with pervaded volume $V_{perv} \approx \langle R_{sc,0}^2\rangle^{3/2} \approx (blN_{sc})^{3/2}$. This pervaded volume can only fit $V_{perv}/V_{sc} \approx (bl)^{3/2} N_{sc}^{1/2}/v$ side chains, each with a physical volume $V_{sc} \approx vN_{sc}$. A section of the backbone of size $\langle R_{sc,0}^2\rangle^{1/2}$ passing through this pervaded volume contains N_{sc} monomers if it is in its unperturbed Gaussian conformation (assuming the same conformational statistics of backbone and side chains). Therefore, if grafting density is too high ($z > z^*$), the $N_{sc}z$ side chains grafted to the undeformed section of the backbone with combined physical volume $vN_{sc}^2 z > V_{perv}$ can no longer fit in the pervaded volume V_{perv}, forcing the backbone to extend.

The backbone extension on the length scale $\langle R_{sc,0}^2\rangle^{1/2}$ assures a fixed number of grafting points along the backbone section of this size $\langle R_{sc,0}^2\rangle^{1/2}$ equal to the number of overlapping side chains $\langle R_{sc,0}^2\rangle^{3/2}/(vN_{sc}) \approx (bl)^{3/2} N_{sc}^{1/2}/v$. On the small length scales, up to the size of the tension blob (*54*), the backbone remains unperturbed. The size of the tension blob $\xi \approx (blg)^{1/2}$ consisting of g monomers is estimated from the condition that gz side chains emanated from this section of the backbone densely fill its pervaded volume ξ^3 [there are $\xi^3/(vg) \approx gz$ such overlapping chain sections]. Therefore, the tension blob size is $\xi \approx (lb)^2/(vz)$. There is no crowding issue on length scales r smaller than the tension blob ($r < \xi$), and bottlebrush backbones maintain the unperturbed Gaussian conformations with bare Kuhn length b. On the intermediate length scales ($\xi < r < \langle R_{sc,0}^2\rangle^{1/2}$),

a backbone can be visualized as an extended array of tension blobs with a constant average distance between grafting points $v/(bl)$. On larger length scales ($r > \langle R^2_{sc,0}\rangle^{1/2}$), backbones of bottlebrushes in a melt are represented as random walks of these extended arrays of tension blobs. The loosely grafted bottlebrush (LB part of Fig. 2) is described as a thick filament with contour length $L \approx N_{bb}vz/(bl)$, thickness equal to the end-to-end distance of its side chains $\langle R^2_{sc,0}\rangle^{1/2}$, and persistence length on the same order of magnitude (see detailed derivation in the subsection "Persistence length of a bottlebrush in a melt"). Thus, bottlebrush macromolecules are considered as chains of $L/\langle R^2_{sc,0}\rangle^{1/2}$ effective monomers of size $\langle R^2_{sc,0}\rangle^{1/2}$. The mean square end-to-end distance of the backbone of an LB

$$\langle R^2\rangle \approx L\langle R^2_{sc,0}\rangle^{1/2} \approx \frac{vz}{(bl)^{1/2}} N_{bb}N_{sc}^{1/2} \qquad z^* < z < z^{**} \qquad (2)$$

increases with increasing degree of polymerization N_{sc} and grafting density z of side chains. Considering bottlebrush as a dense "sausage-like" random walk, we can estimate its mean square size from its physical volume $V_{chain} \approx vzN_{bb}N_{sc}$ as $\langle R^2\rangle \approx V_{chain}/\langle R^2_{sc,0}\rangle^{1/2}$.

Side chains begin to extend at the crossover between loosely grafted and densely grafted bottlebrush regimes (red line in Fig. 2 at $z \approx z^{**}$). The crossover value of the grafting density is given by

$$z^{**} = \frac{l^2 b}{v} \min\left(\frac{b^2 l}{v}, 1\right) \qquad (3)$$

This crossover occurs either if the backbone spacer between neighboring grafting points begins to extend (for $v > b^2l$) or if the backbone approached the fully extended state (for $v < b^2l$). In the former case at $z \approx z^{**} \approx (bl)^3/v^2$, the scale associated with the tension blob of the backbone $\xi \approx (lb)^2/(vz)$ becomes comparable to the unperturbed spacer size $(bl/z)^{1/2}$. At high grafting density ($z^{**} < z < l^{3/2}/v^{1/2}$), the balance of side chain and backbone spacer stretching leads to the equilibrium size of extended side chains $\langle R^2_{sc}\rangle^{1/2} \approx N_{sc}^{1/2} v^{1/3} z^{1/6}$, with the corresponding average spacer length $(v/z)^{1/3}$ and the contour length of the bottlebrush $L_{bb} \approx v^{1/3}z^{2/3}N_{bb}$. The mean square size of the bottlebrush in this regime is

$$\langle R^2\rangle \approx \langle R^2_{sc}\rangle^{1/2} L_{bb} \approx \frac{V_{chain}}{\langle R^2_{sc}\rangle^{1/2}} \approx v^{2/3} z^{5/6} N_{sc}^{1/2} N_{bb}$$

$$\text{for} \quad v > b^2 l \text{ and } \frac{(bl)^3}{v^2} < z < \frac{l^{3/2}}{v^{1/2}} \qquad (4)$$

The backbone is almost fully stretched in the case of lower monomer volume $v < b^2l$ if $z > z^{**} \approx (l^2b)/v$ or, for higher grafting density, $z > l^{3/2}/v^{1/2}$ in the case of higher monomer volume $v > b^2l$. In this case, the dense packing of side chains forces them to extend to the mean square size

$$\langle R^2_{sc}\rangle \approx \frac{vz}{l} N_{sc} \text{ for } z > \frac{l^2 b}{v} \text{ if } v < b^2 l \text{ or}$$

$$\text{for } z > \frac{l^{3/2}}{v^{1/2}} \text{ if } v > b^2 l \qquad (5)$$

The filament-like bottlebrush with both thickness and persistence length on the order of $\langle R^2_{sc}\rangle^{1/2}$ and bottlebrush contour length on the order of the contour of the backbone lN_{bb} has mean square size

$$\langle R^2\rangle \approx (vlzN_{sc})^{1/2} N_{bb} \qquad \text{for} \quad z > \frac{l^2 b}{v} \text{ if } v < b^2 l \text{ or}$$

$$\text{for} \quad z > \frac{l^{3/2}}{v^{1/2}} \quad \text{if} \quad v > b^2 l \qquad (6)$$

The dependence of backbone and side-chain size of combs and bottlebrushes on z is summarized in Fig. 3.

The size of side chains of densely grafted bottlebrushes with almost fully stretched backbones

The size of side chains increases with degree of polymerization N_{sc} (see fig. S1 and table S1). Their size also increases with grafting density z along the backbone. This effect is illustrated in Fig. 4A, which exhibits the variation of the ratio of the mean square distance $\langle R^2_{sc}(s)\rangle$ of side-chain monomer s from the grafting point and the corresponding Gaussian size $s\sigma^2$ as a function of the bond index s for different grafting densities z. Different colors and symbols correspond to bottlebrushes with different values of N_{bb}, N_{SC}, and z, as shown in Fig. 4B and table S2. To understand the bond index s dependence of the mean square distance $\langle R^2_{sc}(s)\rangle$, we consider the average of the square of the size $R_{sc}(s) = \langle R_{sc}(s)\rangle + \delta R_{sc}(s)$ of these side-chain segments containing s monomers

$$\langle R^2_{sc}(s)\rangle = \langle R_{sc}(s)\rangle^2 + \langle \delta R^2_{sc}(s)\rangle \qquad (7)$$

We assume that the nontrivial s dependence of $\langle R^2_{sc}(s)\rangle$ observed in Fig. 4A is due to chain extension $\langle R_{sc}(s)\rangle$, whereas the fluctuations $\langle \delta R^2_{sc}(s)\rangle$ of the size of these s-segments can be described by the mean square size of chain sections containing s monomers of a free linear 16-mer ($z = 0$, red crosses).

For monomers near the free ends of side chains, the mean distance $\langle R_{sc}(s)\rangle$ can be expanded in the Taylor series of the variable $1 - s/N_{sc}$:

$$\langle R_{sc}(s)\rangle = \langle R_{sc}\rangle \left[1 + \sum_{n>0} a_n \left(1 - \frac{s}{N_{sc}}\right)^n\right] \qquad (8)$$

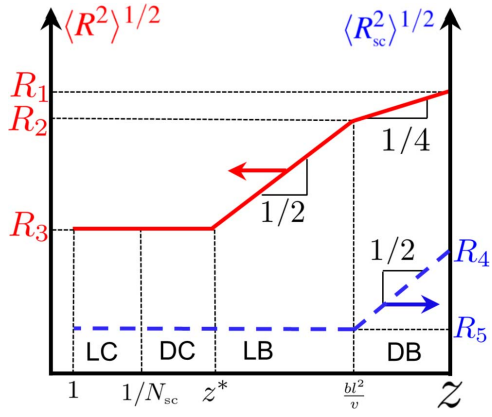

Fig. 3. Size of combs and bottlebrushes in different regimes. With increasing grafting density, the dimensions of both backbone $\langle R^2\rangle^{1/2}$ (red solid line) and side chain $\langle R^2_{sc}\rangle^{1/2}$ (blue dashed line) undergo characteristic variations in the comb (LC and DC) and bottlebrush (LB and DB) regimes. This figure corresponds to the case of lower monomer volume $v < b^2l$. Abbreviations are the same as in Fig. 2. In addition, $R_1 \equiv (vlzN_{sc})^{1/4}N_{bb}^{1/2}$, $R_2 \equiv (l^3bN_{sc})^{1/4}N_{bb}^{1/2}$, $R_3 \equiv (blN_{bb})^{1/2}$, $R_4 \equiv (vz/l)^{1/2}N_{sc}^{1/2}$, and $R_5 \equiv (blN_{sc})^{1/2}$.

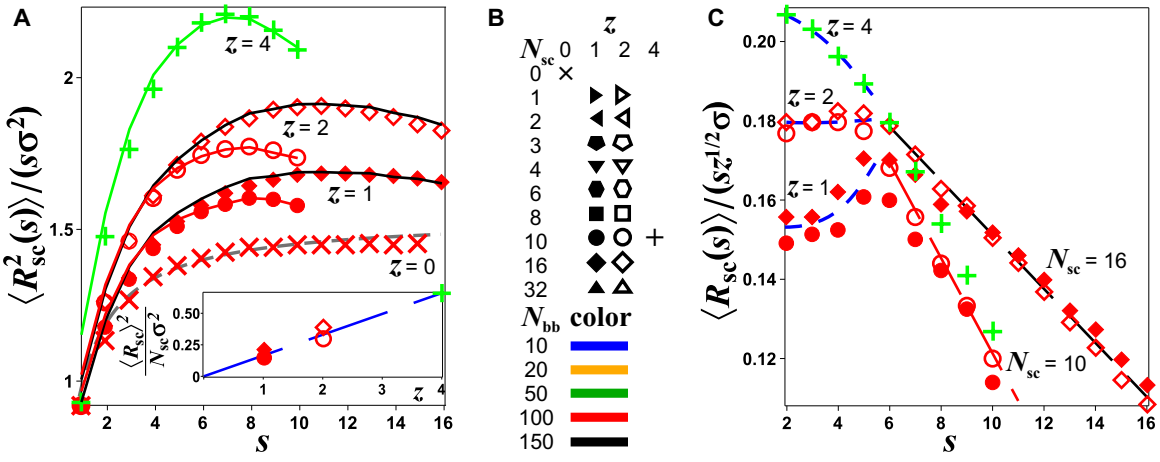

Fig. 4. Size of side chains of bottlebrushes in a melt. (**A**) Dependence of the rescaled values of the mean square distance of a side-chain monomer s from the grafting point $\langle R_{sc}^2(s)\rangle/(s\sigma^2)$ for side chains with N_{sc} = 10 and N_{sc} = 16 monomers as a function of the bond index s counting from the grafting point for molecules with different number z of grafted side chains per backbone monomer. The mean square fluctuations of the size of an s-segment $\langle \delta R_{sc}^2(s)\rangle$ are assumed to be equal to their value for linear 16-mer in a melt (z = 0, crosses). The dashed line is the fit to these z = 0 points by $C_\infty^{lin}/(1+\tilde{s}/s)$ with two adjustable parameters C_∞^{lin} = 1.55 and $\tilde{s}$ = 0.61. Curves for $z \geq 1$ show theoretical predictions of Eq. 10 with fitting parameter $\langle R_{sc}\rangle$. (Inset) Dependence of $\langle R_{sc}\rangle^2/(N_{sc}\sigma^2)$ on parameter z for $\langle R_{sc}\rangle$ obtained from the separate fit to Eq. 10 for each curve. Dashed line represents the theoretical prediction of Eq. 11 with scaling parameter C_{sc} = 0.17. (**B**) Convention of symbols used in all figures to denote a particular bottlebrush melt. Color and shape of symbols denote the values of N_{bb} and N_{sc}, respectively. Crosses represent the data for linear chains (z = 0), solid symbols correspond to bottlebrushes with z = 1, open symbols are for bottlebrushes with z = 2, and plus symbols denote the data for bottlebrushes with z = 4 (see table S2 for more details). (**C**) Dependence of the rescaled values $\langle R_{sc}(s)\rangle/(sz^{1/2}\sigma)$ of the corresponding mean distance $\langle R_{sc}(s)\rangle = [\langle R_{sc}^2(s)\rangle - \langle \delta R_{sc}^2(s)\rangle]^{1/2}$ on the bond index s. Dashed lines are the theoretical predictions (see text for details).

where $\langle R_{sc}\rangle = \langle R_{sc}(N_{sc})\rangle$ is the average size of a side chain. The first coefficient is $a_1 = 0$ due to the boundary condition $dR_{sc}/ds = 0$ at the free end $s = N_{sc}$. The condition $\langle R_{sc}(s)\rangle \ll \langle R_{sc}\rangle$ for small $s \ll N_{sc}$ leads to the constraint for the sum of all coefficients $\Sigma_n a_n = -1$. Note that the asymptotic expressions for the higher-order coefficients a_n in Eq. 8 can be found by expanding the dependence $\langle R_{sc}(s)\rangle \propto (s/N_{sc})^{1/2} = [1-(1-s/N_{sc})]^{1/2}$ (see Eq. 14 below) in the power series of $(1-s/N_{sc})$. Comparing this expansion with expansion in Eq. 8 term by term, we estimate $a_3 \approx -1/16$ and coefficients a_n decay with n as $n^{-3/2}$. The small values of these coefficients justify omission of the higher-order terms in the expansion in Eq. 8. Thus, we take all $a_{n>2} = 0$ and $a_2 = -1$ and obtain

$$\langle R_{sc}(s)\rangle \simeq \frac{s}{N_{sc}}\left(2-\frac{s}{N_{sc}}\right)\langle R_{sc}\rangle \qquad \text{for} \quad \gamma N_{sc} \lesssim s \leq N_{sc} \qquad (9)$$

The parameter $\gamma \sim 0.3$ to 0.5 defines the lower boundary of the interval of validity of the above approximation. The mean square size of linear chain segments containing s monomers $\langle \delta R_{sc}^2(s)\rangle$ obtained from molecular dynamics simulations is presented by the lowest set of points denoted by × symbols in Fig. 4A. This dependence can be approximated by $\langle \delta R_{sc}^2(s)\rangle \simeq s\sigma^2 C_\infty^{lin}/(1+\tilde{s}/s)$, where $C_\infty^{lin} = 1.55$ and $\tilde{s} = 0.61$, as shown by the dashed line (see Eq. 22 below for the similar approximation for bottlebrush backbones). In Fig. 4A, we compare our prediction from Eqs. 7 and 9

$$\frac{\langle R_{sc}^2(s)\rangle}{s\sigma^2} = \frac{s}{N_{sc}}\left(2-\frac{s}{N_{sc}}\right)^2\frac{\langle R_{sc}\rangle^2}{N_{sc}\sigma^2} + \frac{C_\infty^{lin}}{1+\tilde{s}/s}$$

$$\text{for} \quad \gamma N_{sc} \lesssim s \leq N_{sc} \qquad (10)$$

with the data obtained from simulations of bottlebrushes with grafting density z = 1, 2, and 4 using single fitting parameter $\langle R_{sc}\rangle$ and the value of $C_\infty^{lin} = 1.55$ and $\tilde{s} = 0.61$ from the fit to linear chain data (z = 0). This simple estimate (Eq. 10) demonstrates excellent agreement with the simulation data.

The average side-chain size $\langle R_{sc}\rangle$ can be estimated from the monomer dense packing condition. The transverse slice of a bottlebrush can be approximated by a disc of volume $d\langle R_{sc}\rangle^2$ and thickness $d \approx \sigma$ of the backbone bond projection onto the contour of the molecule. Assuming that there is no (or limited) overlap between the side chains of neighboring bottlebrushes, the disc volume is occupied by z side chains of volume vN_{sc} each, where $v \approx \sigma^3$ is the volume of one monomer. Therefore, the square of the average size of side chains can be estimated as

$$\langle R_{sc}\rangle^2 \simeq \frac{vN_{sc}z}{d} = C_{sc}N_{sc}z\sigma^2 \qquad (11)$$

where C_{sc} is the numerical coefficient accounting for the scaling form of this expression. The inset in Fig. 4A shows good agreement with Eq. 11, with the value of the fitting parameter C_{sc} = 0.17.

Combining Eqs. 9 and 11, we can write

$$\langle R_{sc}(s)\rangle \simeq C_{sc}^{1/2}\left(2-\frac{s}{N_{sc}}\right)\frac{s\sigma z^{1/2}}{N_{sc}^{1/2}} \qquad \text{for} \quad \gamma N_{sc} \lesssim s \leq N_{sc} \qquad (12)$$

In Fig. 4C, we test this prediction by plotting the s dependence of the ratio of the average distance $\langle R_{sc}(s)\rangle = [\langle R_{sc}^2(s)\rangle - \langle \delta R_{sc}^2(s)\rangle]^{1/2}$ and $s\sigma z^{1/2}$ using the simulation data presented in Fig. 4A. For larger values of s for $\gamma N_{sc} \lesssim s \leq N_{sc}$, this rescaled function is z-independent and exhibits linear dependence on s, $\langle R_{sc}(s)\rangle/(s\sigma z^{1/2}) \simeq C_{sc}^{1/2}(2-s/N_{sc})/N_{sc}^{1/2}$, with N_{sc}-dependent negative slope predicted by Eq. 12. The red and black dashed lines in Fig. 4C (for $s > 6$) have slopes of −0.012 and −0.0064 for N_{sc} = 10 and N_{sc} = 16, respectively, which are consistent with the predicted negative slopes $-C_{sc}^{1/2}/N_{sc}^{3/2} = -0.013$ and −0.0063 from Eq. 12.

The mean square fluctuations of the size of chain segments containing large number $s \gg 1$ of monomers are Gaussian. Therefore, the normalized mean square size of side-chain segments (Eq. 10) can be approximated for large s by

$$\frac{\langle R_{sc}^2(s)\rangle}{s\sigma^2} = C_{sc}\frac{zs}{N_{sc}}\left(2-\frac{s}{N_{sc}}\right)^2+\frac{C_\infty^{lin}}{1+\tilde{s}/s} \simeq C_{sc}\frac{zs}{N_{sc}}\left(2-\frac{s}{N_{sc}}\right)^2+C_\infty^{lin} \quad \text{for } \gamma N_{sc} \lesssim s \le N_{sc} \tag{13}$$

This equation predicts a maximum at $s_{max} = 2N_{sc}/3$. This prediction is in good agreement with the simulations (see Fig. 4A). Note that the position of the maximum (for both points and lines) has a slightly higher value of s than $2N_{sc}/3$ because of the residual s dependence of the ratio $\langle \delta R_{sc}^2(s)\rangle/(s\sigma^2)$ for short side chains. The physical explanation of this peak is that not all of the chains extend all the way to $\langle R_{sc}\rangle$. There is a wide distribution of the positions of side-chain ends around their average value $\langle R_{sc}\rangle$. Because fewer side chains extend to larger radial distances from the backbone, they provide an additional contribution to the ratio $\langle R_{sc}^2(s)\rangle/(s\sigma^2)$ in Eq. 13 for $\gamma N_{sc} < s < s_{max}$ and a relatively smaller contribution for larger values of $s > s_{max}$. As a result of side chains that do not extend to large radial distances from the backbone, the crowding of remaining side chains at these large radial distances decreases. This decrease in crowding weakens the stretching of the remote side-chain sections, resulting in a relatively smaller average extension of chain sections with $s > 2N_{sc}/3$. The stretching decreases with s and vanishes at the free side-chain ends in the overlapping zone of neighboring bottlebrushes.

Conformations of side-chain segments with $s \lesssim \gamma N_{sc}$ near the grafting point are determined by the monomer packing condition due to the limited penetration of monomers with index $s' > s$ into this zone near the backbone, similar to packing restrictions for the entire side chain (see Eq. 11)

$$\langle R_{sc}(s)\rangle^2 \simeq \frac{zvs}{d} \simeq zs\sigma^2 \quad \text{for} \quad s \lesssim \gamma N_{sc} \tag{14}$$

Therefore, the ratio $\langle R_{sc}(s)\rangle/(s\sigma z^{1/2})$ should be independent of N_{sc} for small $s \lesssim \gamma N_{sc}$, as observed in Fig. 4C. However, note that the s dependence of $\langle R_{sc}(s)\rangle$ for $s \lesssim 6$ differs from our prediction (Eq. 14) because of strong crowding of side-chains near the backbone and the non-Gaussian behavior of these short chain segments. The s dependence of $\langle \delta R_{sc}^2(s)\rangle/(s\sigma^2)$ significantly deviates from a constant for $s \lesssim 6$ (see red crosses in Fig. 4A), as described by the crossover expression $C_\infty^{lin}/(1+\tilde{s}/s)$.

Persistence length of a bottlebrush in a melt

The rigidity of bottlebrush is only due to the mutual repulsion of the crowded side chains. The excluded volume interactions in a melt state are highly screened. In the unrealistic case of complete screening of steric interactions, the resulting persistence length of a bottlebrush is on the order of its monomer size $\approx \sigma$. To estimate the persistence length of "real" bottlebrushes, we have to account for partially screened excluded volume interactions between side chains. The physical volume of $s_p z$ side chains grafted to a persistent bottlebrush section is $vs_p zN_{sc}$, whereas the radius of this section is $\langle R_{sc}^2\rangle^{1/2}$. Therefore, the length of this cylindrical-like section is $vs_p zN_{sc}/\langle R_{sc}^2\rangle$ and its pervaded volume is $\approx (vs_p zN_{sc}/\langle R_{sc}^2\rangle)^3$. The pervaded volume of a persistent bottlebrush section is the volume of a sphere that encompasses this cylindrical-like persistent segment. The excluded volume interactions between polymer sections in the melt are reduced by the degree of polymerization $P_w = s_p zN_{sc}$ of these sections (*54*) (see Fig. 5). Thus, the free energy of the excluded volume interactions between these persistent bottlebrush sections within their pervaded volume is

$$E_{sc} = k_B T \frac{v}{P_w}\frac{(s_p zN_{sc})^2}{(vs_p zN_{sc}/\langle R_{sc}^2\rangle)^3} \tag{15}$$

The persistent segment s_p is determined by the condition that the excluded volume interaction energy E_{sc} is on the order of thermal energy $k_B T$, resulting in

$$s_p \approx \frac{\langle R_{sc}^2\rangle^{3/2}}{vzN_{sc}} \approx \frac{(zvN_{sc})^{1/2}}{d^{3/2}} \tag{16}$$

where Eq. 11 $\langle R_{sc}^2\rangle^{1/2} \approx (zvN_{sc}/d)^{1/2}$ was used. In this case, the size of the persistence segment ℓ_p is

$$\ell_p \approx s_p d \approx \left(\frac{zvN_{sc}}{d}\right)^{1/2} \approx \langle R_{sc}^2\rangle^{1/2} \tag{17}$$

The conformations of bottlebrush backbones at small length scales are similar to those of flexible polyelectrolytes that are almost undeformed on scales up to electrostatic blob size but extended into a linear array of electrostatic blobs on larger length scales with persistence length determined by the screening length (*55*). By analogy with the polyelectrolytes, bottlebrushes are flexible on small length scales and have large persistence length, induced by side-chain repulsion, on intermediate length scales.

Our simulations confirm the scaling prediction that the persistence length of bottlebrush backbones in a melt state is comparable to the size of side chains. To determine the length of persistence segments s_p,

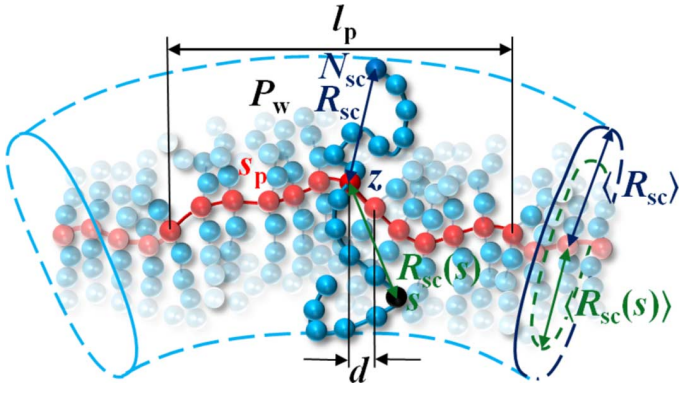

Fig. 5. Geometry of a bottlebrush polymer. A bottlebrush is composed of z side chains with N_{sc} monomers each grafted to every backbone monomer ($z = 2$ in this figure). $R_{sc} \equiv R_{sc}(N_{sc})$ and $R_{sc}(s)$ denote instantaneous values of size of side chains (bottlebrush thickness) and distance of a side-chain monomer s from the grafting point, respectively. The number of monomers per persistence segment is s_p, and persistence length is ℓ_p. $P_w \approx s_p zN_{sc}$ is the total degree of polymerization of cylindrical-like section composed of s_p backbone monomers and $s_p zN_{sc}$ side-chain monomers. d is average projection of a backbone bond onto the direction of the backbone contour.

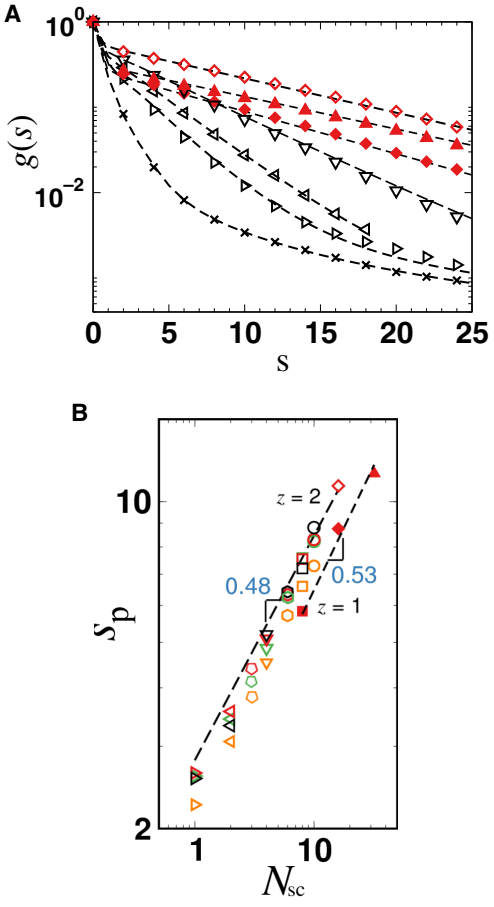

Fig. 6. Persistence segment of a bottlebrush in a melt. (**A**) Decay of backbone bond orientational correlations $g(s)$ as a function of the number of monomers s between two bonds for bottlebrushes with various degrees of polymerization N_{sc} of side chains and number z of side chains grafted per backbone monomer (see Fig. 4B and the corresponding caption for the definition of symbols). Dashed lines represent best fits to the expression for $g(s)$ given by Eq. 18. (**B**) Persistence segments obtained from the decay of bond orientational correlations plotted as a function of the side-chain polymerization degree N_{sc} for various backbones N_{bb} and grafting densities z of side chains, as indicated. The dashed lines represent the best power-law fit for data sets with $N_{bb} = 100$: $s_p = 1.91N_{sc}^{0.53\pm0.04}$ for $z = 1$ and $s_p = 2.75N_{sc}^{0.48\pm0.03}$ for $z = 2$.

we calculated the decay rate of the correlations between bond orientations $g(s) \equiv \langle \cos\theta \rangle \propto e^{-s/s_p}$ (see simulation data in Fig. 6A and fig. S2). The cosine of the angle is $\cos\theta = (\mathbf{r}_i/|\mathbf{r}_i|) \cdot (\mathbf{r}_{i+s}/|\mathbf{r}_{i+s}|)$, where $\mathbf{r}_i = \mathbf{R}_{i+1} - \mathbf{R}_i$ is the bond vector i between monomers i and $i + 1$, and $\mathbf{r}_{i+s} = \mathbf{R}_{i+s+1} - \mathbf{R}_{i+s}$ is the bond vector $i + s$ between monomers $i + s$ and $i + s + 1$. The data obtained from simulations (symbols) have been fitted to the function (dashed lines) of the following form

$$g(s) = (1 - A)e^{-s/s_f} + Ae^{-s/s_p} + \zeta s^{-3/2} \tanh\left[(s/3)^3\right] \qquad (18)$$

where A, s_f, s_p, and ζ are fitting parameters (see table S3) and denote the following: $(1 - A)$ and A are the magnitudes of short- and long-range correlations, respectively, between bond vectors of the backbone; s_f is the characteristic number of beads in the backbone, which undergo "local" bond vector correlations; s_p is the number of beads per persistence segment; and ζ is the magnitude of long-range interactions induced by the connectivity of backbone bonds (see the section on persistence length in the Supplementary Materials for details). The power-law decay $\propto s^{-3/2}$ at $s \gg 1$ was reported for polymers melts (*56*) and for θ solutions (*57*). The origin of these interactions is explained either by effective compression of polymer coils due to the correlation hole effect (*56*) or by the shift of the monomeric Mayer *f*-function due to the finite interaction range and chain connectivity (*57*). The function $\tanh[(s/3)^3]$ presented in Eq. 18 describes a cutoff at minimal loop size $s = 3$.

In Fig. 6B, the number of monomers along the bottlebrush backbone in the persistent segment s_p is presented as a function of the degree of polymerization of side chains N_{sc} for grafting densities $z = 1$ and 2 and various backbone degrees of polymerization N_{bb}. These data demonstrate the effect of backbone straightening with the increasing N_{sc} and z. The exponents of the observed power laws

$$s_p = 1.91N_{sc}^{0.53\pm0.04} \quad \text{for} \quad z = 1 \qquad (19)$$

$$s_p = 2.75N_{sc}^{0.48\pm0.03} \quad \text{for} \quad z = 2 \qquad (20)$$

agree with the exponent $1/2$ predicted from the scaling arguments, as presented in the beginning of this subsection (see Eq. 16), and indicate that the number of monomers s_p in the persistence segments of the bottlebrush backbones with $z = 1$ or 2 side chain per backbone monomer and $N_{bb} \gtrsim 50$ is proportional to the brush radius (side-chain size $\langle R_{sc}^2 \rangle^{1/2}$) (see fig. S3).

Size of a bottlebrush in a melt

The size of a bottlebrush in a melt state can be estimated from a simple physical picture of nonoverlapping flexible filaments with $\ell_p \propto \langle R_{sc}^2 \rangle^{1/2}$. Consider a bottlebrush backbone that is much longer than persistence segment $N_{bb} \gg s_p$ (see Fig. 1B). The bottlebrush conformation can be represented as a chain of effective monomers consisting of s_p backbone monomers and $s_p z$ side chains of size $\langle R_{sc}^2 \rangle^{1/2}$. The mean square end-to-end distance of the backbone can be estimated as the number of these effective monomers N_{bb}/s_p times the square of their size, which is proportional to the mean square size of side chains $\langle R_{sc}^2 \rangle$, resulting in $\langle R^2 \rangle \approx \langle R_{sc}^2 \rangle N_{bb}/s_p$. Because the number of monomers in a persistence segment s_p is proportional to the size of a side chain $\langle R_{sc}^2 \rangle^{1/2} \approx \sigma N_{sc}^{1/2}$ (see Eqs. 17, 19, and 20), we predict that the mean square size of the backbone is also proportional to the size of a side chain $\langle R^2 \rangle \approx \sigma \langle R_{sc}^2 \rangle^{1/2} N_{bb} = \sigma^2 N_{bb} N_{sc}^{1/2}$. Our simulation results corroborate this prediction (cf. Eq. 6), as discussed below.

The mean square end-to-end distance of the backbone $\langle R^2 \rangle$ and the mean square radius of gyration $\langle R_g^2 \rangle$ of the whole bottlebrush are plotted as functions of the degree of polymerization of side chains N_{sc} and backbone N_{bb} in Fig. 7 and fig. S4 (for the definition of symbols, see Fig. 4B and the corresponding caption as well as table S2). The mean square size increases with N_{bb} and N_{sc} and obeys the power law

$$\begin{aligned} \langle R^2 \rangle / N_{bb} &= 1.33N_{sc}^{0.47\pm0.01}\,\sigma^2 \quad \text{for} \quad z = 1 \\ \langle R^2 \rangle / N_{bb} &= 2.76N_{sc}^{0.47\pm0.01}\,\sigma^2 \quad \text{for} \quad z = 2 \end{aligned} \qquad (21)$$

and $\langle R_g^2 \rangle / N_{bb} = 0.23N_{sc}^{0.49\pm0.01}\,\sigma^2$ for $z = 1$ and $\langle R_g^2 \rangle / N_{bb} = 0.46N_{sc}^{0.47\pm0.01}\,\sigma^2$ for $z = 2$. Similar to linear chains in melts, the

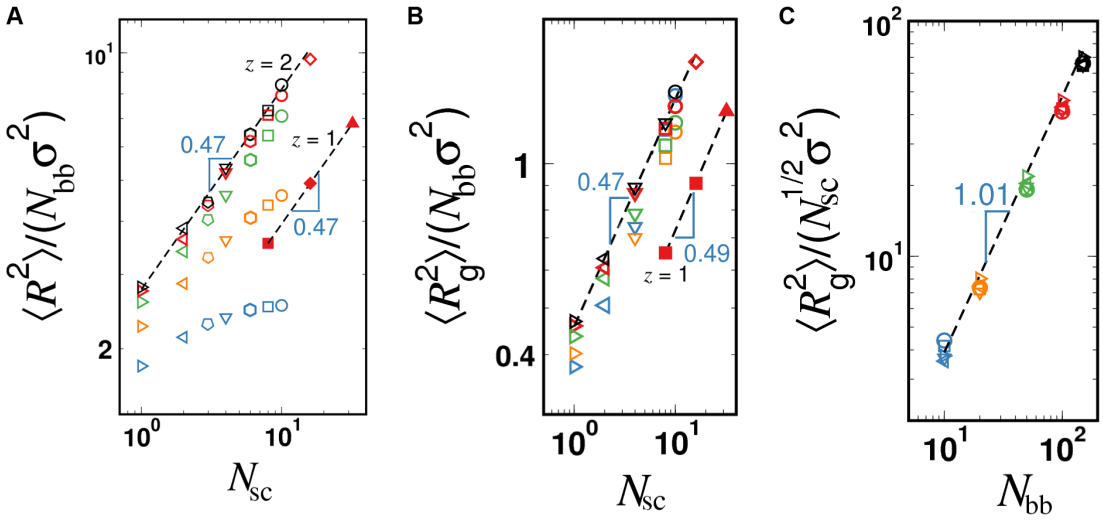

Fig. 7. Size of bottlebrushes in a melt. Mean square end-to-end distance $\langle R^2\rangle$ (**A**) and mean square radius of gyration $\langle R_g^2\rangle$ (including side chains) (**B**) of bottlebrushes in a melt normalized by the ideal mean square size of backbones $N_{bb}\sigma^2$ as functions of the degree of polymerization of side chains N_{sc}. (**C**) Mean square radius of gyration $\langle R_g^2\rangle$ of bottlebrushes normalized by σ times the ideal root mean square size of side chains $N_{sc}^{1/2}\sigma^2$ as a function of the degree of polymerization of backbones N_{bb}. See Fig. 4B and the corresponding caption for the definition of symbols. In (A) and (B), the number of side chains grafted per backbone monomer is $z = 1$ and 2. (C) displays data for $z = 2$. Dashed lines represent fitted scaling laws: (A) $1.33N_{sc}^{0.47\pm0.01}$ for $z = 1$ and $N_{bb} = 100$ and $2.76N_{sc}^{0.47\pm0.01}$ for $z = 2$ and $N_{bb} = 100$, (B) $0.23N_{sc}^{0.49\pm0.01}$ for $z = 1$ and $N_{bb} = 100$ and $0.46N_{sc}^{0.47\pm0.01}$ for $z = 2$ and $N_{bb} = 100$, and (C) $0.39N_{bb}^{1.01\pm0.04}$ for $z = 2$ and $N_{sc} = 10$. The error bars for all data points are smaller than the size of symbols.

conformations of bottlebrushes with long backbones are well described by the ideal chain statistics, that is, $\langle R^2\rangle/\langle R_g^2\rangle \approx 6$, as verified by the distributions of the end-to-end distances R and the radii of gyration R_g (cf. fig. S5). From Fig. 7A, one can observe that the mean square end-to-end distance of molecules with backbones $N_{bb} = 10$ and 20 becomes insensitive to further increase in N_{sc}. This is attributed to the crossover from the crew-cut bottlebrushes to the starlike configurations.

The mean square internal distances $\langle R^2(s)\rangle$ between backbone monomers are plotted in Fig. 8 as a function of the number of bonds s in a backbone section for molecules with various side-chain degrees of polymerization N_{sc} and different number z of side chains grafted per backbone monomer (the definition of symbols is displayed in Fig. 4B and described in the corresponding caption). The simulation data for all z values were fitted to the crossover expression

$$\langle R^2(s)\rangle = s\sigma^2 \frac{C_\infty^{bb}}{1+\tilde{s}/s} \qquad (22)$$

with fitting parameters C_∞^{bb} and $\tilde{s}$ plotted in Fig. 8B and reported in table S4. The overall good agreement between the crossover expression and simulation data is observed by the overlap between points (simulation data) and lines (Eq. 22) in Fig. 8A. The backbone stretching (characterized by both parameters C_∞^{bb} and $\tilde{s}$) increases significantly with the grafting density of side chains z and with the degree of polymerization of side chains N_{sc} because of steric repulsion between densely grafted side chains. The Flory characteristic ratio C_∞^{bb} and parameter $\tilde{s}$ increase proportionally to the power of the degree of polymerization of side chains $C_\infty^{bb} = 1.3N_{sc}^{0.52\pm0.01}$ and $\tilde{s} = 2.1N_{sc}^{0.51\pm0.1}$ for $z = 1$ and $C_\infty^{bb} = 2.8N_{sc}^{0.53\pm0.01}$ and $\tilde{s} = 3.4N_{sc}^{0.55\pm0.01}$ for $z = 2$ (see Fig. 8B and table S4). The scaling exponents are close to $^1/_2$, indicating that s dependence of distances between backbone bonds separated by s monomers for $s > \tilde{s}$ is consistent with the backbone size scaling (Eq. 21). We observe that $\tilde{s}$ is 60% and 25% larger than corresponding C_∞^{bb} values (see

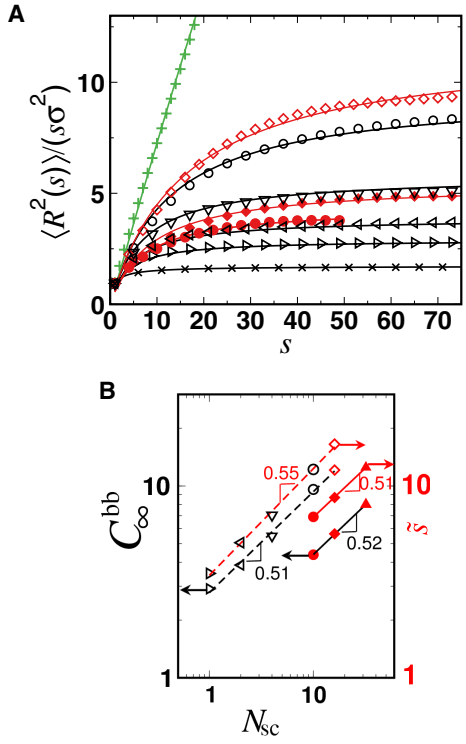

Fig. 8. Extension of a bottlebrush in a melt. (**A**) Dependence of the mean square internal distances $\langle R^2(s)\rangle$ between bottlebrush backbone monomers normalized by their ideal mean square size $s\sigma^2$ on the number of monomers s in the backbone sections plotted for various side-chain polymerization degrees N_{sc} and grafting densities z (see Fig. 4B and its caption for the definition of symbols). Solid lines represent best fits to the crossover expression $\langle R^2(s)\rangle/(s\sigma^2) = \frac{C_\infty^{bb}}{1+\tilde{s}/s}$, with fitting parameters C_∞^{bb} and $\tilde{s}$ listed in table S4. (**B**) Fitting parameters C_∞^{bb} and $\tilde{s}$ plotted as a function of side-chain polymerization degree N_{sc} for $z = 1$ (full symbols) and $z = 2$ (open symbols). Dashed lines represent fitted scaling laws: $C_\infty^{bb} = 1.3N_{sc}^{0.52\pm0.01}$ and $\tilde{s} = 2.1N_{sc}^{0.51\pm0.01}$ for $z = 1$, whereas $C_\infty^{bb} = 2.8N_{sc}^{0.53\pm0.01}$ and $\tilde{s} = 3.4N_{sc}^{0.55\pm0.01}$ for $z = 2$.

Fig. 8B and table S4) for $z = 1$ and 2, respectively, pointing out the wiggling of the backbone $\langle R^2(s)\rangle^{1/2} \approx s^{1/2}\,\sigma$ on length scales smaller than the tension blob. The bottlebrushes undergo a conformational transformation from a random coil to a rod as the grafting density z increases from 1 to 4, which is evidenced by the increase of both the Flory characteristic ratio C_∞^{bb} and the crossover value $\tilde{s}$ by more than an order of magnitude. Because the backbone degree of polymerization $N_{bb} \ll \tilde{s}$, the simulated bottlebrush with side-chain grafting density $z = 4$ is effectively rodlike. Note that it is hardly possible to determine persistence segment s_p from correlations of bond orientations (see Eq. 18) for simulated bottlebrushes with short backbones $N_{bb} \lesssim 50$ and $z = 4$ because the corresponding $g(s)$ functions do not decay sufficiently.

Interpenetration of neighboring bottlebrushes in a melt

As discussed below, reduced interpenetration of side chains from neighboring macromolecules is a distinct feature that distinguishes segregated filaments (bottlebrushes) from overlapped molecules (linear chains and combs). This interpenetration is crucial for the understanding of the friction between these molecules and for the explanation of the complex rheological response of bottlebrush-based materials observed in recent experiments (*12*, *26*, *27*, *58*, *59*). We have analyzed the number of intramolecular h_s and intermolecular g_s contacts between side-chain monomers. Contacts were defined between pairs of monomers within distance $r_{shell} = 1.5\sigma$ from each other. This separation corresponds to the position of the minimum in the interbead correlation function $g(r)$, as discussed below. We denote by $\langle h_s\rangle$ the average number of intramolecular nonbonded contacts between sth monomer of a side chain and monomers within the same host molecule, whereas $\langle g_s\rangle$ stands for the average number of intermolecular contacts between the ith monomer of a side chain of a given molecule with monomers belonging to all other molecules. Both quantities were calculated as functions of monomer index s along a side chain and normalized by the average number of nonbonded neighbors per sth monomer $Z_s = \langle h_s\rangle + \langle g_s\rangle$. The average value of Z_s is independent of the monomer index s, $Z_s \approx \langle Z\rangle \approx 4.7$, except for terminal monomers $Z_1 \approx 5.0$ and $Z_{N_{sc}} \approx 5.3$. The results of this analysis are presented in Fig. 9A (for the definition of symbols, see Fig. 4B and the corresponding caption as well as table S2). The average fraction of intermolecular contacts for the first side-chain monomers ($s = 1$) is low and decreases with increasing grafting density z: $\langle g_1\rangle/\langle Z_1\rangle \approx 0.2$ for $z = 1$, $\langle g_1\rangle/\langle Z_1\rangle \approx 0.1$ for $z = 2$, and $\langle g_1\rangle/\langle Z_1\rangle < 0.01$ for $z = 4$. The limited interpenetration is ascribed to dense crowding of the side-chain monomers belonging to the same bottlebrush in the vicinity of its backbone, which hinders penetration of guest monomers to the central region of the host bottlebrush. The probability of encountering guest monomers $\langle g_s\rangle/\langle Z_s\rangle$ increases with s and reaches the maximum value for terminal monomers of the side chains. This maximum value was found to be $\langle g_{N_{sc}}\rangle/\langle Z_{N_{sc}}\rangle \approx 1/2$ independent of grafting density z and degree of polymerization of side chains N_{sc}. The terminal monomers are in the interpenetration zone between two neighboring bottlebrushes. This zone contains 50:50 composition of monomers from both molecules. The low interpenetration of bottlebrushes in a melt state is demonstrated by the "territorial map" (*60*–*62*) of the simulation box snapshot in Fig. 9B.

For a reference system, we have calculated the number of contacts between monomers of neighboring linear chains in a melt (cf. the inset of Fig. 9A). The interchain contacts for linear polymers are almost uniformly distributed along the backbone except for the chain ends. The estimated fraction of guest monomers for linear chains was found to be $\langle g_s\rangle/\langle Z_s\rangle \approx 0.65$ (independent of the degree of polymerization) and is higher than the maximum fraction of 0.5 (encountered by end monomers of bottlebrush side chains). The increase in the fraction of intermolecular contacts of up to ≈ 0.78 is observed at the ends of linear chains. The intrachain nonbonded contacts in linear chains are due to the formation of self-loops. For inner monomers of a linear chain, one can have self-loops at both sides, whereas for end monomers, self-loops can only be formed from one side. This explains the higher number of interchain contacts for end monomers of linear chains in a melt. The main conclusion of this analysis is that the overlap of bottlebrush molecules in the melt is qualitatively different on a monomer level from that of linear chains. Below, we show that melts of bottlebrushes become qualitatively similar to those of linear chains if we describe bottlebrushes as thick flexible filaments, which are chains of "effective monomers" of size $\langle R_{sc}^2\rangle^{1/2}$.

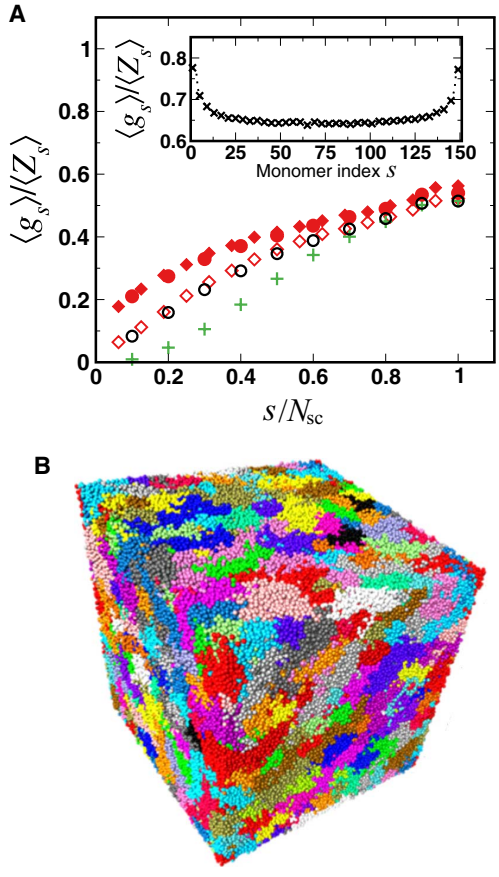

Fig. 9. Interpenetration of bottlebrushes in a melt. (**A**) Average number of contacts $\langle g_s\rangle$ between bottlebrush side-chain monomer s and monomers of other molecules. The value of $\langle g_s\rangle$ is normalized by the average number of nonbonded neighbors $\langle Z_s\rangle$ and plotted as a function of monomer index i (counting from the backbone) normalized by the degree of polymerization of side chains N_{sc}. Data for $N_{sc} = 10$ and $N_{sc} = 16$, with grafting density $z = 1$, 2, and 4 of side chains per backbone monomer (see Fig. 4B and the corresponding caption for the definition of symbols). The inset displays the average number of contacts $\langle g_s\rangle$ between sth monomer of a linear chain and monomers of surrounding linear chains in a melt normalized by the average number of nonbonded neighbors. (**B**) The "map of territories" for an equilibrated melt of bottlebrushes with $N_{bb} = 100$, $N_{sc} = 10$, and $z = 2$ demonstrates reduced overlap between neighboring molecules.

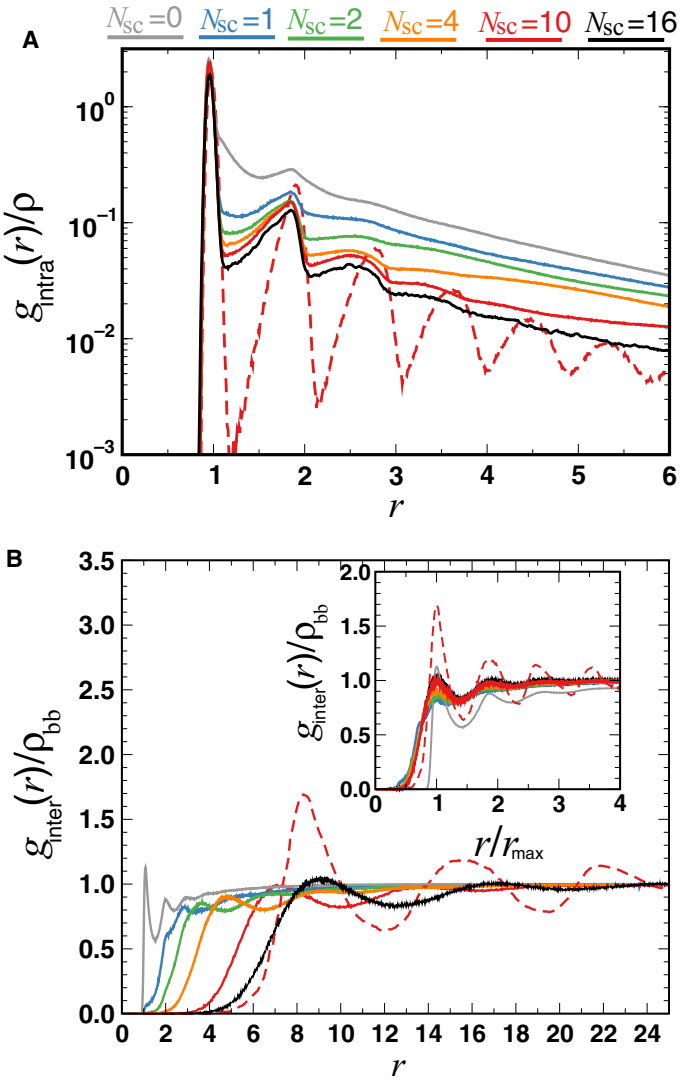

Fig. 10. Radial distribution function of bottlebrushes in a melt. Pair correlation functions between (**A**) intrabackbone monomers $g_{intra}(r)$ and (**B**) interbackbone monomers $g_{inter}(r)$ normalized by melt density ρ and density of backbone monomers in a melt ρ_{bb}, respectively. Correlation functions were plotted for various degrees of polymerization of side chains N_{sc}. As indicated in the legend, various colors are used to distinguish between the lines with different values of N_{sc}. Solid gray lines denote results for linear melts, that is, with grafting density $z = 0$ ($N_{sc} = 0$), whereas other solid lines correspond to $z = 2$. Dashed lines represent results for $z = 4$ and $N_{sc} = 10$.

Local structure

The internal structure of melts composed of linear chains or bottlebrushes is illustrated in Fig. 10 by the pair correlation functions $g(r)$ of backbone monomers. The intrabackbone pair correlation function $g_{intra}(r)$ has several peaks, as shown in Fig. 10A, for both linear chains and bottlebrush melts with different side-chain grafting densities z. There are two peaks in melts of bottlebrushes with short side chains: one at $r \approx 0.96$ σ that corresponds to bonded (nearest) neighbors and the peak at $r \approx 1.87$ σ that corresponds to second-nearest neighbors. As the degree of polymerization of side chains N_{sc} increases, one observes that, for the grafting density of $z = 2$ side chains per backbone monomer (solid lines), new peaks appear at $r \approx 2.6$ σ and 3.4 σ, which are due to stretching of the backbone. As the number of side chains attached to a backbone monomer increases to $z = 4$ (dashed line), the backbone stiffens and more peaks appear, indicating stronger intramolecular correlations. In this case, a series of clearly distinguishable subsequent and equidistant maxima is observed: 1.92σ, 2.79σ, 3.63σ, 4.48σ, 5.32σ, … The existence of local structure for bottlebrush melts is due to long-range interactions between backbone monomers induced by side chains. The strength of the intramolecular interaction increases with grafting density z and with length of side chains. The longer the side chains are, the stronger the interaction is between backbone monomers and the longer the range of these interactions is. The interaction range along the backbone is comparable to the size of the persistence segment, which scales with the size of side chains as $\langle R_{sc}^2 \rangle^{1/2}$.

The information about bottlebrush packing in the melt is contained in the interbackbone correlation function $g_{inter}(r)$ presented in Fig. 10B. In the case of linear chain melts, $g_{inter}(r)$ reveals the structure at very small length scales. $g_{inter}(r)$ is zero for distances r below first peak because of Lennard-Jones (LJ) core repulsion between monomers. The sharp peak at $r \approx 1.1$ σ corresponds to the first "solvation shell," which is the optimal distance between pairs of nearest-neighbor monomers. The second peak at $r \approx 1.9$ σ displays the influence from the shell of the second-nearest neighbors. In contrast to melts of linear chains, the large-scale structure is observed in bottlebrush melts. Bottlebrush backbones are shielded by densely grafted side chains and do not approach each other. This fact is clearly demonstrated in the case of bottlebrushes with the long side chains, that is, $N_{sc} = 10$ (solid red line for $z = 2$ and dashed red line for $z = 4$). At distances comparable to bottlebrush thickness, equal to the average side-chain size $\langle R_{sc}^2 \rangle^{1/2} \approx 4.18$ σ for $z = 2$ and at $\langle R_{sc}^2 \rangle^{1/2} \approx 4.58$ σ for $z = 4$, the corresponding values of $g_{inter}(r)$ are low $g_{inter}(r)/\rho_{bb} \approx 0.1$ because the "coat" of side chains around a given backbone prevents neighboring backbones from approaching it. Note that the highest probability to find monomers of neighboring backbones does not exactly match the brush diameter $2\langle R_{sc}^2 \rangle^{1/2}$ but is rather at a shorter distance because of partial interpenetration of side chains. The first maxima are observed at $r_{max} \approx 7.25$ σ for $z = 2$ and ≈ 8.35 σ for $z = 4$, respectively. The smaller value of $r_{max}/(2\langle R_{sc}^2 \rangle^{1/2})$ for $z = 2$ (≈0.87) with respect to $z = 4$ (≈0.91) implies a stronger overlap of grafted side chains in bottlebrush melts with lower z (see Fig. 9). The inset of Fig. 10B shows the correlation functions $g_{inter}(r)$, with the abscissa rescaled by the position of the first maximum r_{max}. The positions of the peaks for bottlebrush systems correlate very well with the peaks observed for linear chain, indicating a similar "liquid-like" origin of melt structure (*63*, *64*) but with stronger correlations at correspondingly larger distances. This result justifies representing bottlebrushes in melts by chains of "effective" monomers of size $\propto \langle R_{sc}^2 \rangle^{1/2}$, which are thick flexible filamentous objects.

The form factor of a bottlebrush backbone in a melt

The form factor $S(q)$ of the backbones of bottlebrushes with different grafting densities z of side chains is presented as the Holtzer plot in Fig. 11. The form factor of linear chains ($z = 0$) in a melt state (solid black line) is well represented by the Debye function (black dashed line) and scales as $S(q) \propto q^{-2}$ for large wave vectors q. The backbone form factors of bottlebrushes exhibit different behavior because of the backbone extension induced by side chains. For bottlebrushes with $z = 2$ (solid red line), the backbone $S(q)$ at intermediate values of wave vector $q < 0.5\ \sigma^{-1}$ is similar to the form factor of a semiflexible chain. The simulation data for $z = 2$ (solid red line) were fitted to the theoretical prediction of the structure factor of a semiflexible chain (blue

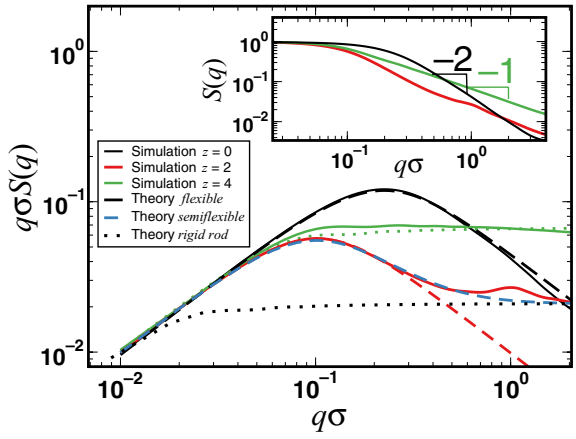

Fig. 11. The form factor of a bottlebrush in a melt. The Holtzer representation of the backbone form factor of bottlebrush melts with different grafting densities of side chains per backbone monomer $z = 2$ (red solid line) and $z = 4$ (green solid line). The black solid line represents the form factor of a linear chain ($z = 0$). The blue dashed line depicts the theoretical prediction for the form factor of a semiflexible chain (*65*). The dotted lines (black and green) represent form factors of a rigid rod, whereas black and red dashed lines are Debye form factors of a flexible chain. The inset shows simulation data in the standard, $S(q)$ versus q, representation. The scaling laws of the ideal chain $\propto q^{-2}$ for $z = 0$ and the rigid rod $\propto q^{-1}$ for $z = 4$ are denoted.

dashed line) (*65*). Note that the form factor of a semiflexible chain (blue dashed line) interpolates between the Debye function (red dashed line) at large length scales (small q values) and rigid rod form factor (dotted black line) at small length scales (high q values). The overall very good agreement between simulation data and theoretical prediction (*65*) is observed. The only difference is the presence of a hump located between $q \approx 0.65\ \sigma^{-1}$ and $1.96\ \sigma^{-1}$. The nonmonotonicity of Holtzer plot $qS(q)$ for high q values is attributed to the local flexibility of bottlebrushes at small length scales. Flexibility of bottlebrushes at length scales below tension blob size ξ is also confirmed by the existence of the fast initial decay of backbone bond correlations (see Fig. 6A and Eq. 18). The case of bottlebrushes with $z = 4$ (solid green line) cannot be fitted by the theoretical structure factor of a semiflexible chain. Larger crowding of side-chain monomers around the backbone gives rise to its increased extension for bottlebrushes with $z = 4$. The persistence length in this case is much larger than bottlebrush thickness, and structure factor is well approximated by the rigid rod–like scattering (dotted green line).

DISCUSSION

The conformations of bottlebrush macromolecules in melts depend on the side-chain grafting density z and the degree of polymerization of side chains N_{sc}. We demonstrated that the increase of z and N_{sc} leads to the extension of the bottlebrush backbone at intermediate length scales and enhancement of long-range interactions between backbone monomers, causing stronger intra- and intermolecular correlations similar to semidilute polyelectrolyte solutions. These interactions also result in significant reduction of the overlap between side chains of neighboring molecules. For moderate grafting densities with $z \leq 2$, the conformation of bottlebrush is similar to a filament composed of "effective monomers" of size comparable with bottlebrush thickness (size of side chains). The bottlebrush size follows ideal (Gaussian) chain statistics for $z \leq 2$, and the mean square size of a bottlebrush is proportional to the product of the backbone degree of polymerization N_{bb} and the persistence length of the molecule $\propto N_{sc}^{1/2}$, that is, $\langle R^2 \rangle \propto N_{bb} N_{sc}^{1/2}$. For high grafting densities $z > 3$, bottlebrushes with short backbones $N_{bb} \lesssim 50$ adopt rodlike conformations.

MATERIALS AND METHODS

Simulations of bottlebrush melts were performed using three-dimensional coarse-grained bead-spring model (*63*). An individual bottlebrush molecule is composed of N_{bb} backbone monomers (beads) connected by bonds and z side chains of N_{sc} monomers grafted to every backbone monomer (see Fig. 1A). Thus, the total number of beads in a bottlebrush is $N = N_{bb} + zN_{bb}N_{sc}$, where z is the grafting density. The case of $N_{sc} = 0$ (or $z = 0$) corresponds to a linear chain.

The nonbonded interactions between monomers separated by distance r were modeled by the truncated and shifted LJ potential

$$V^{LJ}(r) = \begin{cases} 4\epsilon[(\sigma/r)^{12} - (\sigma/r)^6 + (\sigma/r_c)^6 - (\sigma/r_c)^{12}] & r \leq r_c \\ 0 & r > r_c \end{cases} \quad (23)$$

where the interaction strength ϵ is measured in units of thermal energy $k_B T$, σ is the monomer diameter, and r_c is the cutoff. In the NVT ensemble, we have used $\epsilon = k_B T$ and $r_c = 2^{1/6}\sigma$. This choice of LJ potential results in purely repulsive interactions between monomers. The bonded interactions in a molecule were described by the Kremer-Grest potential (*63*), $V^{KG}(r) = V^{FENE}(r) + V^{LJ}(r)$, with the "finitely extensible nonlinear elastic" (FENE) potential

$$V^{FENE} = -\frac{1}{2} k r_0^2 \ln\left[1 - \left(\frac{r}{r_0}\right)^2\right] \quad (24)$$

where the bond stiffness $k = 30\ \epsilon/\sigma^2$ and the maximum bond length $r_0 = 1.5\ \sigma$ (*63*). All simulations were performed in a cubic box with periodic boundary conditions imposed in all spatial dimensions. In the NVT ensemble, the simulations were carried out at the overall monomer density $\rho = 0.85\ \sigma^{-3}$ corresponding to the intermolecular pressure $\langle P \rangle \approx 4.75\ \epsilon/\sigma^3$. In a separate set of simulations, we have also investigated melts of bottlebrushes with attractive LJ potential with the interaction strength $\epsilon = 0.84\, k_B T$ and the cutoff $r_c = 2.5\ \sigma$ using NPT ensemble with $P = 0$, ensuring that the average density $\langle \rho \rangle \approx 0.85\ \sigma^{-3}$ is the same as in the NVT runs. The static properties obtained from both NVT and NPT simulations, for example, the average bottlebrush size, demonstrate good agreement with each other within the error bars after rescaling by the corresponding average bond length l (bonds in NPT simulations are 1% shorter than those in NVT simulations).

The molecular dynamics simulations were performed by solving the Langevin equation of motion for the position $\mathbf{r}_i = [x_i, y_i, z_i]$ of each bead (*66*)

$$m\ddot{\mathbf{r}}_i = \mathbf{F}_i^{LJ} + \mathbf{F}_i^{FENE} - \zeta \dot{\mathbf{r}}_i + \mathbf{F}_i^{R},\ i = 1, \ldots, N \quad (25)$$

which describes the motion of a set of interacting monomers. Forces $\mathbf{F}_i^{LJ}$ and $\mathbf{F}_i^{FENE}$ in Eq. 25 above are obtained from the LJ (Eq. 23) and FENE

(Eq. 24) interaction potentials between the ith monomer and surrounding monomers. The third and fourth terms on the right-hand side of Eq. 25 are a slowly evolving viscous force $-\zeta\dot{\mathbf{r}}_i$ and a rapidly fluctuating stochastic force $\mathbf{F}_i^{\mathrm{R}}$, respectively. This random force $\mathbf{F}_i^{\mathrm{R}}$ is related to the friction coefficient ζ by the fluctuation-dissipation theorem $\langle \mathbf{F}_i^{\mathrm{R}}(t)\mathbf{F}_j^{\mathrm{R}}(t')\rangle = k_{\mathrm{B}}T\zeta\delta_{ij}\delta(t-t')$. The friction coefficient used in simulations was $\zeta = 0.5\ m\tau^{-1}$, where m is the monomer mass and $\tau = \sqrt{m\sigma^2/\epsilon}$ is the LJ time. The velocity Verlet scheme (*67*) was used for numerical integration of equations of motion in Eq. 25. The integration step was taken to be $\Delta\tau = 0.01\tau$. A Langevin thermostat was used to keep the temperature constant. All simulations were carried out using Large-scale Atomic/Molecular Massively Parallel Simulator (LAMMPS) (*68*). Simulation snapshots were rendered using Visual Molecular Dynamics (VMD) (*69*). Initially, molecules were grown using a self-avoiding random walk technique and placed randomly in the simulation cell. The initial density of all systems was small ($\approx 0.03\ \sigma^{-3}$). Overlapping monomers in the initial configuration were pushed off using soft potential with slowly ramped interaction strength. To obtain the desired melt density ($\rho = 0.85\ \sigma^{-3}$), the simulation box was gradually decreased in size (see fig. S6) at constant velocity $10^{-3}\sigma/\tau$. Equivalently, a short ($\approx 10^4\tau$) NPT simulation was performed at pressure $P = 0.01\epsilon/\sigma^3$. We have verified that the results do not depend on the sample preparation method. Once the target density was reached, simulations were continued for up to at least three relaxation times of the corresponding system. During the equilibration stage, the molecules diffused, on average, at least the root mean square end-to-end distance of their backbones.

Simulations of bottlebrush and linear chain melts were carried out for the following number of backbone monomers $N_{\mathrm{bb}} = 10$, 16, 20, 50, 100, and 150. The number of side-chain monomers N_{sc} was varied between 0 and 32 for bottlebrushes with $z = 1$ and between 0 and 16 for bottlebrushes with $z = 2$ side chains attached to each backbone monomer. We assign unique symbols to denote data for each particular system. The convention of symbols used throughout the article is displayed in Fig. 4B. The complete list of symbols can be found in table S2. In addition, for molecules with $N_{\mathrm{bb}} = 50$, the number of side chains per backbone monomer was varied ($z = 0$, 1, 2 and 4). To avoid the finite size effects, the number of molecules M in a simulation box was changed; thus, the box size a was at least ≈ 2.5 times larger than the root mean square end-to-end distance $\langle R^2\rangle^{1/2}$ of bottlebrush backbones. Table S2 summarizes all parameters used in our computer simulations.

SUPPLEMENTARY MATERIALS

Supplementary material for this article is available at http://advances.sciencemag.org/cgi/content/full/2/11/e1601478/DC1

The size of a bottlebrush side chains in a melt

Persistence length of a bottlebrush in a melt

The size of a bottlebrush in a melt

Bottlebrush melt preparation

table S1. Summary of the adjustable parameters C_∞^{sc} and $\tilde{N}_{\mathrm{sc}}$ describing the mean square size of side chains.

table S2. Summary of system parameters for simulations of bottlebrush melts and linear chain melts.

table S3. Summary of the adjustable parameters A, s_{f}, s_{p}, and ζ for the bond angle correlation function.

table S4. Parameters C_∞^{bb} and $\tilde{s}$ describing the sizes of backbone sections.

fig. S1. The size of side chains of a bottlebrush in a melt.

fig. S2. The bond angle correlation functions $g(s)$.

fig. S3. Persistent segments of bottlebrushes in a melt.

fig. S4. The size of backbones for bottlebrushes in a melt.

fig. S5. Distribution of sizes of bottlebrushes in a melt.

fig. S6. A scheme demonstrating sample preparation of a bottlebrush melt.

fig. S7. Snapshots displaying conformations of bottlebrush molecules in a melt state.

REFERENCES AND NOTES

1. K. L. Beers, S. G. Gaynor, K. Matyjaszewski, S. S. Sheiko, M. Möller, The synthesis of densely grafted copolymers by atom transfer radical polymerization. *Macromolecules* **31**, 9413–9415 (1998).
2. Z. Li, K. Zhang, J. Ma, C. Cheng, K. L. Wooley, Facile syntheses of cylindrical molecular brushes by a sequential RAFT and ROMP "grafting-through" methodology. *J. Polym. Sci. A Polym. Chem.* **47**, 5557–5563 (2009).
3. S. Jha, S. Dutta, N. B. Bowden, Synthesis of ultralarge molecular weight bottlebrush polymers using Grubbs' catalysts. *Macromolecules* **37**, 4365–4374 (2004).
4. Y. Xia, B. D. Olsen, J. A. Kornfield, R. H. Grubbs, Efficient synthesis of narrowly dispersed brush copolymers and study of their assemblies: The importance of side chain arrangement. *J. Am. Chem. Soc.* **131**, 18525–18532 (2009).
5. M. Zhang, A. H. E. Müller, Cylindrical polymer brushes. *J. Polym. Sci. A Polym. Chem.* **43**, 3461–3481 (2005).
6. A. D. Schlüter, J. P. Rabe, Dendronized polymers: Synthesis, characterization, assembly at interfaces, and manipulation. *Angew. Chem. Int. Ed.* **39**, 864–883 (2000).
7. L. Shu, A. Schäfer, A. D. Schlüter, Dendronized polymers: Increasing of dendron generation by the attach-to approach. *Macromolecules* **33**, 4321–4328 (2000).
8. F. Vögtle, S. Gestermann, R. Hesse, H. Schwierz, B. Windisch, Functional dendrimers. *Prog. Polym. Sci.* **25**, 987–1041 (2000).
9. N. Hadjichristidis, M. Pitsikalis, S. Pispas, H. Iatrou, Polymers with complex architecture by living anionic polymerization. *Chem. Rev.* **101**, 3747–3792 (2001).
10. H. Xu, F. C. Sun, D. G. Shirvanyants, M. Rubinstein, D. Shabratov, K. L. Beers, K. Matyjaszewski, S. S. Sheiko, Molecular pressure sensors. *Adv. Mater.* **19**, 2930–2934 (2007).
11. A. Nese, N. V. Lebedeva, G. Sherwood, S. Averick, Y. Li, H. Gao, L. Peteanu, S. S. Sheiko, K. Matyjaszewski, pH-responsive fluorescent molecular bottlebrushes prepared by Atom Transfer Radical polymerization. *Macromolecules* **44**, 5905–5910 (2011).
12. T. Pakuła, Y. Zhang, K. Matyjaszewski, H.-i. Lee, H. Boerner, S. Qin, G. C. Berry, Molecular brushes as super-soft elastomers. *Polymer* **47**, 7198–7206 (2006).
13. L.-H. Cai, T. E. Kodger, R. E. Guerra, A. F. Pegoraro, M. Rubinstein, D. A. Weitz, Soft poly (dimethylsiloxane) elastomers from architecture-driven entanglement free design. *Adv. Mater.* **27**, 5132–5140 (2015).
14. A. Kano, T. Yamano, S. W. Choi, A. Maruyama, Polymer brush-stabilized Polyplex for a siRNA carrier with long blood circulatory half-life. *Adv. Mater. Res.* **47–50**, 762–764 (2008).
15. J. A. Johnson, Y. Y. Lu, A. O. Burts, Y.-H. Lim, M. G. Finn, J. T. Koberstein, N. J. Turro, D. A. Tirrell, R. H. Grubbs, Core-clickable PEG-*branch*-azide bivalent-bottle-brush polymers by ROMP: Grafting-through and clicking-to. *J. Am. Chem. Soc.* **133**, 559–566 (2011).
16. Y. Q. Yang, X. D. Guo, W. J. Lin, L. J. Zhang, C. Y. Zhang, Y. Qian, Amphiphilic copolymer brush with random pH-sensitive/hydrophobic structure: Synthesis and self-assembled micelles for sustained drug delivery. *Soft Matter* **8**, 454–464 (2012).
17. Y. Kamikawa, T. Kato, H. Onouchi, D. Kashiwagi, K. Maeda, E. Yashima, Helicity induction on a poly(phenylacetylene) bearing a phosphonate residue by chiral dendrons. *J. Polym. Sci. A Polym. Chem.* **42**, 4580–4586 (2004).
18. S. Panyukov, E. B. Zhulina, S. S. Sheiko, G. C. Randall, J. Brock, M. Rubinstein, Tension amplification in molecular brushes in solutions and on substrates. *J. Phys. Chem. B* **113**, 3750–3768 (2009).
19. S. V. Panyukov, S. S. Sheiko, M. Rubinstein, Amplification of tension in branched macromolecules. *Phys. Rev. Lett.* **102**, 148301 (2009).
20. J. Paturej, L. Kuban, A. Milchev, T. A. Vilgis, Tension enhancement in branched macromolecules upon adhesion on a solid substrate. *Europhys. Lett.* **97**, 58003 (2012).
21. S. S. Sheiko, F. C. Sun, A. Randall, D. Shirvanyants, M. Rubinstein, H.-i. Lee, K. Matyjaszewski, Adsorption-induced scission of carbon–carbon bonds. *Nature* **440**, 191–194 (2006).
22. A. Milchev, J. Paturej, V. G. Rostiashvili, T. A. Vilgis, Thermal degradation of adsorbed bottle-brush macromolecules: A molecular dynamics simulation. *Macromolecules* **44**, 3981–3987 (2011).
23. M. Wintermantel, M. Schmidt, Y. Tsukahara, K. Kajiwara, S. Kohjiya, Rodlike combs. *Macromol. Rapid Commun.* **15**, 279–284 (1994).
24. S. Namba, Y. Tsukahara, K. Kaeriyama, K. Okamoto, M. Takahashi, Bulk properties of multibranched polystyrenes from polystyrene macromonomers: Rheological behavior I. *Polymer* **41**, 5165–5171 (2000).
25. D. Neugebauer, Y. Zhang, T. Pakuła, S. S. Sheiko, K. Matyjaszewski, Densely-grafted and double-grafted PEO brushes via ATRP. A route to soft elastomers. *Macromolecules* **36**, 6746–6755 (2003).

26. M. Hu, Y. Xia, G. B. McKenna, J. A. Kornfield, R. H. Grubbs, Linear rheological response of a series of densely branched brush polymers. *Macromolecules* **44**, 6935–6943 (2011).
27. W. F. M. Daniel, J. Burdyńska, M. Vatankhah-Varnoosfaderani, K. Matyjaszewski, J. Paturej, M. Rubinstein, A. V. Dobrynin, S. S. Sheiko, Solvent-free, supersoft and superelastic bottlebrush melts and networks. *Nat. Mater.* **15**, 183–189 (2016).
28. T. M. Birshtein, O. V. Borisov, Y. B. Zhulina, A. R. Khokhlov, T. A. Yurasova, Conformations of comb-like macromolecules. *Polym. Sci. U.S.S.R.* **29**, 1293–1300 (1987).
29. G. H. Fredrickson, Surfactant-induced lyotropic behavior of flexible polymer solutions. *Macromolecules* **26**, 2825–2831 (1993).
30. N. A. Denesyuk, Conformational properties of bottle-brush polymers. *Phys. Rev. E* **67**, 051803 (2003).
31. O. V. Borisov, E. B. Zhulina, T. M. Birshtein, Persistence length of dendritic molecular brushes. *ACS Macro Lett.* **1**, 1166–1169 (2012).
32. I. I. Potemkin, Persistence length of comblike polymers strongly adsorbed on a flat surface. *Macromolecules* **39**, 7178–7180 (2006).
33. S. Lecommandoux, F. Chécot, R. Borsali, M. Schappacher, A. Deffieux, A. Brûlet, J. P. Cotton, Effect of dense grafting on the backbone conformation of bottlebrush polymers: Determination of the persistence length in solution. *Macromolecules* **35**, 8878–8881 (2002).
34. S. Rathgeber, T. Pakuła, A. Wilk, K. Matyjaszewski, K. L. Beers, On the shape of bottle-brush macromolecules: Systematic variation of architectural parameters. *J. Chem. Phys.* **122**, 124904 (2005).
35. D. Vlassopoulos, G. Fytas, B. Loppinet, F. Isel, P. Lutz, H. Benoit, Polymacromonomers: Structure and dynamics in nondilute solutions, melts, and mixtures. *Macromolecules* **33**, 5960–5969 (2000).
36. H.-P. Hsu, W. Paul, S. Rathgeber, K. Binder, Characteristic length scales and radial monomer density profiles of molecular bottle-brushes: Simulation and experiment. *Macromolecules* **43**, 1592–1601 (2010).
37. J. Bolton, J. Rzayev, Tandem RAFT-ATRP synthesis of polystyrene–poly(methyl methacrylate) bottlebrush block copolymers and their self-assembly into cylindrical nanostructures. *ACS Macro Lett.* **1**, 15–18 (2012).
38. S. S. Sheiko, B. S. Sumerlin, K. Matyjaszewski, Cylindrical molecular brushes: Synthesis, characterization, and properties. *Prog. Polym. Sci.* **33**, 759–785 (2008).
39. L. Feuz, P. Strunz, T. Geue, M. Textor, O. Borisov, Conformation of poly(L-lysine)-graft-poly (ethylene glycol) molecular brushes in aqueous solution studied by small-angle neutron scattering. *Eur. Phys. J. E* **23**, 237–245 (2007).
40. S. L. Pesek, X. Li, B. Hammouda, K. Hong, R. Verduzco, Small-angle neutron scattering analysis of bottlebrush polymers prepared via grafting-through polymerization. *Macromolecules* **46**, 6998–7005 (2013).
41. M. Saariaho, O. Ikkala, I. Szleifer, I. Erukhimovich, G. ten Brinke, On lyotropic behavior of molecular bottle-brushes: A Monte Carlo computer simulation study. *J. Chem. Phys.* **107**, 3267–3276 (1997).
42. M. Saariaho, I. Szleifer, O. Ikkala, G. ten Brinke, Extended conformations of isolated molecular bottle-brushes: Influence of side-chain topology. *Macromol. Theor. Simul.* **7**, 211–216 (1998).
43. A. Subbotin, M. Saariaho, O. Ikkala, G. ten Brinke, Elasticity of comb copolymer cylindrical brushes. *Macromolecules* **33**, 3447–3452 (2000).
44. H.-P. Hsu, W. Paul, K. Binder, Structure of bottle-brush polymers in solution: A Monte Carlo test of models for the scattering function. *J. Chem. Phys.* **129**, 204904 (2008).
45. H.-P. Hsu, W. Paul, K. Binder, Conformational studies of bottle-brush polymers absorbed on a flat solid surface. *J. Chem. Phys.* **133**, 134902 (2010).
46. H.-P. Hsu, W. Paul, K. Binder, Standard definitions of persistence length do not describe the local "intrinsic" stiffness of real polymer chains. *Macromolecules* **43**, 3094–3102 (2010).
47. H.-P. Hsu, W. Paul, K. Binder, Estimation of persistence lengths of semiflexible polymers: Insight from simulations. *Polym. Sci. Ser. C* **55**, 39–59 (2013).
48. S. Elli, F. Ganazzoli, E. G. Timoshenko, Y. A. Kuznetsov, R. Connolly, Size and persistence length of molecular bottle-brushes by Monte Carlo simulations. *J. Chem. Phys.* **120**, 6257–6267 (2004).
49. L. Feuz, F. A. M. Leermakers, M. Textor, O. Borisov, Bending rigidity and induced persistence length of molecular bottle brushes: A self-consistent-field theory. *Macromolecules* **38**, 8891–8901 (2005).
50. P. E. Theodorakis, H.-P. Hsu, W. Paul, K. Binder, Computer simulation of bottle-brush polymers with flexible backbone: Good solvent versus theta solvent conditions. *J. Chem. Phys.* **135**, 164903 (2011).
51. G. M. Leuty, M. Tsige, G. S. Grest, M. Rubinstein, Tension amplification in tethered layers of bottle-brush polymers. *Macromolecules* **49**, 1950–1960 (2016).
52. Y. Rouault, O. V. Borisov, Comb-branched polymers: Monte Carlo simulation and scaling. *Macromolecules* **29**, 2605–2611 (1996).
53. N. G. Fytas, P. E. Theodorakis, Molecular dynamics simulations of single-component bottle-brush polymers with flexible backbones under poor solvent conditions. *J. Phys. Condens. Matter* **25**, 285105 (2013).
54. M. Rubinstein, R. H. Colby, *Polymer Physics* (Oxford Univ. Press, 2003).
55. A. V. Dobrynin, M. Rubinstein, Theory of polyelectrolytes in solutions and at surfaces. *Prog. Polym. Sci.* **30**, 1049–1118 (2005).
56. J. P. Wittmer, H. Meyer, J. Baschnagel, A. Johner, S. Obukhov, L. Mattioni, M. Müller, A. N. Semenov, Long range bond-bond correlations in dense polymer solutions. *Phys. Rev. Lett.* **93**, 147801 (2004).
57. D. Shirvanyants, S. Panyukov, Q. Liao, M. Rubinstein, Long-range correlations in a polymer chain due to its connectivity. *Macromolecules* **41**, 1475–1485 (2008).
58. C. R. López-Barrón, P. Brant, A. P. R. Eberle, D. J. Crowther, Linear rheology and structure of molecular bottlebrushes with short side chains. *J. Rheol.* **59**, 865–883 (2015).
59. S. J. Dalsin, M. A. Hillmyer, F. S. Bates, Linear rheology of polyolefin-based bottlebrush polymers. *Macromolecules* **48**, 4680–4691 (2015).
60. K. J. Meaburn, T. Misteli, Cell biology: Chromosome territories. *Nature* **445**, 379–381 (2007).
61. T. Cremer, M. Cremer, Chromosome territories. *Cold Spring Harbor Perspect. Biol.* **2**, a003889 (2010).
62. J. R. Dixon, S. Selvaraj, F. Yue, A. Kim, Y. Li, Y. Shen, M. Hu, J. S. Liu, B. Ren, Topological domains in mammalian genomes identified by analysis of chromatin interactions. *Nature* **485**, 376–380 (2012).
63. K. Kremer, G. S. Grest, Dynamics of entangled linear polymer melts: A molecular dynamics simulation. *J. Chem. Phys.* **92**, 5057–5086 (1990).
64. K. G. Honnell, J. G. Curro, K. S. Schweizer, Local structure of semiflexible polymer melts. *Macromolecules* **23**, 3496–3505 (1990).
65. A. L. Kholodenko, Analytical calculation of the scattering function for polymers of arbitrary flexibility using the Dirac propagator. *Macromolecules* **26**, 4179–4183 (1993).
66. M. P. Allen, D. J. Tildesley, *Computer Simulations of Liquids* (Oxford Univ. Press, 1989).
67. L. Verlet, Computer "experiments" on classical fluids. I. Thermodynamical properties of Lennard-Jones molecules. *Phys. Rev.* **159**, 98–103 (1967).
68. S. Plimpton, Fast parallel algorithms for short-range molecular dynamics. *J. Comput. Phys.* **117**, 1–19 (1995).
69. W. Humphrey, A. Dalke, K. Schulten, VMD: Visual molecular dynamics. *J. Mol. Graph.* **14**, 33–38 (1996).

Acknowledgments: J.P. would like to thank J. Brock, A. Erbas, A. Galuschko, M. Koch, T. Kreer, P. Lorchat, M. Mateyisi, O. Sariyer, and J.-U. Sommer for many stimulating discussions. **Funding:** J.P. acknowledged the support from the Polish Ministry of Science and Higher Education (Iuventus Plus: IP2012 005072 and IP2015 059074) and the computational time at PL-Grid. M.R. would like to acknowledge financial support from the NSF (under grants DMR-1122483, DMR-1309892, DMR-1436201, and DMR-1121107), the NIH (under grants P01-HL108808 and 1UH2HL123645), and the Cystic Fibrosis Foundation. S.S. acknowledged the support by NSF under grant DMR-1407645. **Author contributions:** All authors designed and conceived the research. All authors wrote the manuscript. **Competing interests:** The authors declare that they have no competing interests. **Data and materials availability:** All data needed to evaluate the conclusions in the paper are present in the paper and/or the Supplementary Materials. Additional data and materials related to this paper may be requested from the authors and are available online.

Submitted 29 June 2016
Accepted 12 October 2016
Published 11 November 2016
10.1126/sciadv.1601478

Citation: J. Paturej, S. S. Sheiko, S. Panyukov, M. Rubinstein, Molecular structure of bottlebrush polymers in melts. *Sci. Adv.* **2**, e1601478 (2016).

Molecular structure of bottlebrush polymers in melts

Jaros#aw PaturejSergei S. SheikoSergey PanyukovMichael Rubinstein

Sci. Adv., 2 (11), e1601478. • DOI: 10.1126/sciadv.1601478